

# Incrementally Stochastic and Accelerated Gradient Information mixed Optimization for Manipulator Motion Planning

Feng Yichang, Wang Jin\*, Zhang Haiyun, Lu Guodong

**Abstract**—This paper introduces a novel motion planning algorithm, incrementally stochastic and accelerated gradient information mixed optimization (iSAGO), for robotic manipulators in a narrow workspace. Primarily, we propose the overall scheme of iSAGO integrating the accelerated and stochastic gradient information for an efficient constrained optimization based on the penalty method. In the stochastic part, we generate the adaptive stochastic moment via the random selection of collision checkboxes, interval time-series, and penalty factor based on the adaptive momentum (Adam) method to solve the body-obstacle stuck case. Due to the slow convergence of the stochastic part, we integrate the accelerated gradient descent (AGD) to improve the planning efficiency. Moreover, we adopt the Bayesian tree inference (BTI) to transform the whole trajectory optimization (SAGO) into an incremental sub-trajectory optimization (iSAGO), which improves the computation efficiency and success rate. Finally, we tune the key parameters and benchmark iSAGO against other planners (CHOMP, GPMP2, TrajOpt, STOMP, and RRT-Connect) on LBR-iiwa in a bookshelf and AUBO-i5 in a storage shelf. The result shows the highest success rate and moderate solving efficiency of iSAGO.

## I. INTRODUCTION

The industrial robot has been widely applied in various areas such as welding and products loading or placing. The industrial robot always executes the above tasks under manual teaching or programming. So automatic production urges an efficient and robust optimal motion planning (OMP) algorithm to elevate industrial intelligence.

Many former OMP studies gain a collision-free optimal trajectory via numerical optimization [1]–[4] or probabilistic sampling [5]–[10]. However, there still exist two main concerns this paper aims to solve:

(1) Reliability: The numerical methods, such as CHOMP [1], GPMP [2], and TrajOpt [3], can rapidly converge to a minimum with descent steps informed by the deterministic momenta/gradients. However, the local minima (i.e., failure plannings) are unavoidable with an inappropriate initial point. That is because the momenta information only describes the manifold of a local space near the initial point. So it is difficult for them to plan a safe motion with a high success rate (i.e., high reliability) in a narrow space.

(2) Efficiency: The sampling method like STOMP [8] directly samples the trajectories to gain the optima. Others like RRT-Connect [7] construct a probabilistic roadmap by

the randomly generated waypoints. Their sampling process comprehensively gathers the manifold information. However, the searching efficiency highly depends on the proportion the feasible subspace takes of the overall searching space. So the indiscriminate process takes enormous computation resources (i.e., low efficiency) in a narrow space.

So iSAGO integrates the accelerated and stochastic information of momentum and builds a Bayes tree to make an incremental planning:

(1) **Stochastic trajectory optimization with moment adaptation (STOMA)** could overcome the local minimum mainly from the body-obstacle stuck case via the random variable selection, such as collision-check boxes, time intervals, and penalty factors. The information leakage of the stochastic momenta can somewhat modify the manifold of the planning problem with fewer local minima.

(2) Considering the  $\mathcal{O}(\log N/N)$  convergence rate (i.e., low efficiency) of STOMA, iSAGO integrates **accelerated gradient descent (AGD)** in the non-stuck case because its  $\mathcal{O}(1/N^{\frac{3}{2}})$  convergence rate of gradient norm is proven optimal in the first-order convex optimization. Moreover, iSAGO adopts Bayes tree inference to **optimize the trajectory incrementally**, further elevating the efficiency. Because it separately optimizes the convex or non-convex sub-planning problems from the whole trajectory.

The experiment of the 12 planning tasks on LBR-iiwa and AUBO-i5 validates a higher success rate of iSAGO than the numerical methods [1]–[3] and its higher efficiency than the sampling methods [7], [8].

## II. RELATED WORKS

### A. Numerical Optimization

The main concern of numerical optimization is rapidly descending to an optimum. CHOMP [1] and GPMP [2] adopt the gradient descent method with the fixed step size. CHOMP uses Hamiltonian Monte Carlo (HMC) [11] for success rate improvement. To lower the computational cost, GPMP and dGPMP [4] adopt iSAM2 [12] to do incremental planning and each sub-planning converges with super-linear rate via Levenberg–Marquardt (LM) [13] algorithm. Moreover, TrajOpt [3] uses the trust-region [14] method to expedite motion planning. Nevertheless, the above methods may guide the trajectory into the local minima when the objective function is not strongly convex.

Accelerated gradient descent (AGD) [15], [16] has recently been developed and implemented on the optimal control [17], [18] of a dynamic system described by differential equations whenever the objective is strongly convex or not.

\* Wang Jin, corresponding author, 1) State Key Laboratory of Fluid Power and Mechatronic Systems, School of Mechanical Engineering, Zhejiang University, Hangzhou 310027, China; 2) Engineering Research Center for Design Engineering and Digital Twin of Zhejiang Province, School of Mechanical Engineering, Zhejiang University, Hangzhou 310027, China. dwjcom@zju.edu.cn

Moreover, stochastic optimization employs the momentum theorems of AGD and solves the large-scale semi-convex cases [19], which generates stochastic sub-gradient via the random sub-datasets selection. Adam [20] upgrades RMSPProp [21] and introduces an exponential moving average (EMA) for momentum adaptation. Furthermore, [22] adopts Adam to overcome the disturbance of a UAV system.

### B. Probabilistic Sampling

Unlike the numerical method, the sampling method constructs a roadmap or samples trajectory for motion planning.

PRM [5], including its upgrade like PRM\* [9] and RRGs [23]), makes a collision-free connection among the feasible vertexes to construct a roadmap. Then they construct an optimal trajectory via the all-pairs short paths (APSPs) methods like Dijkstra [24] and Chehov [25] algorithm, which stores and queries partial trajectories efficiently. Unlike PRM associated with APMPs, RRT [6], including its upgrade like RRT\* [9] and CODEs [10], find a feasible solution by growing rapidly-exploring random trees (RRTs).

STOMP [8] resamples trajectory obeying Gaussian distribution renewed by the important samples. [26] introduces the GPMP's function to improve the searching efficiency of STOMP. Moreover, SMTO [27] applies Monte-Carlo optimization for multi-solution and refines them numerically.

## III. PROBLEM FORMULATION

### A. Objective functional

This paper adopts the objective functional proposed in CHOMP [1] and GPMP [2] to generate an optimal trajectory in high smoothness without collision. In this way, we design the objective functional of trajectory  $\theta$  as:

$$\mathcal{F}(\theta) = \varrho \mathcal{F}_{gp}(\theta) + \mathcal{F}_{obs}(\theta) \quad (1)$$

where  $\varrho$  trades off between a Gaussian process (GP) prior

$$\mathcal{F}_{gp}(\theta) = \frac{1}{2} (\theta - \mu)^\top \mathcal{K}^{-1} (\theta - \mu), \quad (2)$$

where  $\mu$  and  $\mathcal{K}$  denote the expectation and the covariance of GP-distribution  $\mathcal{GP}(\mu, \mathcal{K})$ , and an obstacle functional

$$\mathcal{F}_{obs}(\theta) = \sum_{t \in \mathbf{T}} \sum_{\mathcal{B}_i \in \mathcal{B}} c[\mathbf{x}(\mathcal{B}_i, t)] \cdot \|\dot{\mathbf{x}}(\mathcal{B}_i, t)\|, \quad (3)$$

where  $\mathbf{T} = \{t_1, \dots, t_2\}$  contains the timestamps of support waypoints from  $t_1$  to  $t_2$ ,  $\mathcal{B} = \{\mathcal{B}_1, \dots, \mathcal{B}_{N_B}\}$  consists of  $N_B$  collision-check boxes (CCBs), and  $c(\cdot) : \mathbb{R}^3 \rightarrow \mathbb{R}$  calculates the collision cost whose value increases when shrinking the distance between CCB- $\mathcal{B}_i$  and its closest obstacle. In addition, our incremental method utilizes  $\mathbf{T} = \{t_1, \dots, t_2\}$  to extract the sub-trajectory within  $[t_1, t_2]$  from the whole trajectory (i.e.,  $\mathbf{T} = \{t_0, \dots, t_g\}$ ), and Section III-B details how to construct a Bayes tree by  $\mathbf{T}$ .

Moreover, the up-sampling [2] method is adopted for time-continuous safety. According to the Gauss-Markov model <sup>1</sup>

<sup>1</sup>Section 4 of [2] introduces the GP-prior, Gauss-Markov model generated by a linear time-varying stochastic differential equation (LTV-SDE), and GP-interpretation utilized by Section 5.3 for up-sampling.

$\Phi(t_{i+1}, t_i)$ , transforming  $\theta(t_i)$  to  $\theta(t_{i+1})$ , we get

$$\Lambda_{i,\tau} = \Phi(t_i + \frac{\tau}{n_i^p} \Delta t_i, t_i) - \Psi_{i,\tau} \Phi(t_{i+1}, t_i), \quad (4)$$

$$\Psi_{i,\tau} = \mathbf{Q}_{i,\tau} \Phi(t_{i+1}, t_i + \frac{\tau}{n_i^p} \Delta t_i)^\top \mathbf{Q}_{i,i+1}^{-1}. \quad (5)$$

where  $\Delta t_i = t_{i+1} - t_i$  and  $\mathbf{Q}_{i,\tau}$  transforms the covariance from  $t_i$  to  $(t_i + \frac{\tau}{n_i^p} \Delta t_i)$ . The above methods are utilized by (14) to generate the stochastic momenta in the time scale.

### B. Bayes tree construction

The Bayes tree (BT) of a trajectory is a single chain because its conjugated waypoints are correlated in time series. According to the objective functional in (1), we first decompose the whole trajectory into discrete serial waypoints to gain a set of BT-nodes  $\Theta = \{\theta_0, \dots, \theta_g\}$ . Then we gain the BT-branch by connecting any two adjacent nodes  $\{\theta_i, \theta_{i+1}\}$  in the time series. In this way, the BT-factor

$$\mathcal{F}_i = \mathcal{F}[\theta(t_{i-1}, t_{i+1})] \text{ with } \mathbf{T} = \{t_{i-1}, t_i, t_{i+1}\} \quad (6)$$

of a BT-node  $\theta_i \in \Theta$  is calculated according to (1) and (3).

## IV. METHODOLOGY

### A. incrementally Stochastic and Accelerated Gradient information mixed for trajectory Optimization

Given the initial and goal waypoints, iSAGO (Algorithm 1, Figure 1) first interpolates the support waypoints between them via the GP-based Bayes inference to gain an initial trajectory. Then it finds a series of collision-free waypoints facing the two planning scenarios: (i) the convex case satisfying (9); (ii) the non-convex case where the trajectory gets stuck in obstacles, leading to a local minimum.

Given these two cases, iSAGO mixes the accelerated and stochastic gradient information. AGD (Section IV-B) solve case (i) with an optimal convergence informed by the first order accelerated gradient. On the other hand, STOMA (Section IV-C) utilizes the stochastic gradient to drag the trajectory from the case (ii) into a convex sub-space, a.k.a. case (i). Moreover, iSAGO uses the penalty method [28] to nest the above methods in *PenIter* for constrained optimization.

Formally, the mixed gradient descent optimizes the whole trajectory to plan a safe motion. However, it is inefficient because the whole trajectory consists of collision-free, in-collision, and in-stuck parts, each requiring different methods. So we adopt iSAM2 [12] to build a Bayes tree (Figure 1) with factors informed by the sub-functional (6) of each support waypoint. Since an optimal Bayes tree does not have a significant factor, incremental-SAGO (iSAGO) finds significant factors and optimizes them incrementally in *iSAGO.reTrajIter*. To sift out the significant, we compute the mean value and standard deviation of BT factors (6) by

$$\mu_{\mathcal{F}} = \sum_{i \in [1, N_g]} w_i \mathcal{F}_i, \quad \mathcal{D}_{\mathcal{F}} = \sqrt{\sum_{i \in [1, N_g]} w_i (\mathcal{F}_i - \mu_{\mathcal{F}})^2}, \quad (7)$$

where  $w_i = 1/N_g$  and  $N_g$  is the number of waypoints. Next, iSAGO gains a set of waypoints with significant factors:

$$\Theta_{\mathfrak{N}} = \{\theta_i \mid \|\mathcal{F}(\theta_i) - \mu_{\mathcal{F}}\| > c_{\eta} \mathcal{D}_{\mathcal{F}}\}, \quad (8)$$

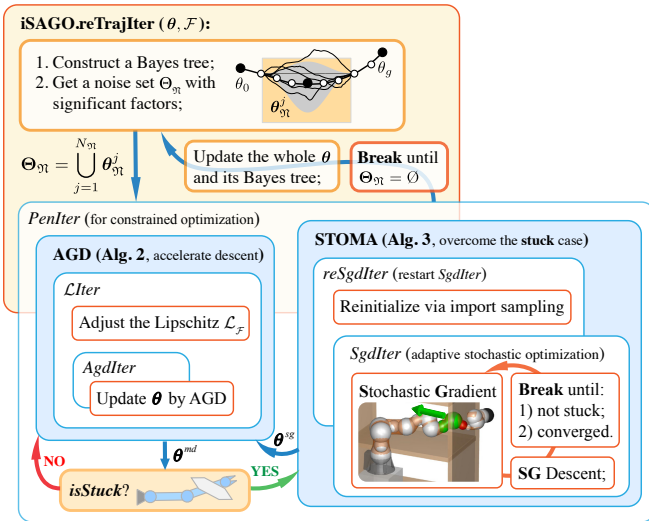


Fig. 1: A block diagram illustrates iSAGO (Algorithm 1, Section IV-A) does collision-free OMP, whose outer layer shows how to refine a whole trajectory via BTI-based sub-trajectories optimization. The *PenIter* integrates AGD (Algorithm 2, Section IV-B) and STOMA (Algorithm 3, Section IV-C) to solve the non-convex OMP by detecting the stuck case.

---

### Algorithm 1: iSAGO

---

**Input:** initial trajectory  $\theta$ ,  $\mathcal{GP}$ -distribution, Bayes tree, and tradeoff coefficient  $\varrho$ .

**for** *reTrajIter* :  $i = 1 \dots N_{uf}$  **do**

  Get noisy set  $\Theta_{\mathcal{N}} = \bigcup_{j=1}^{N_{\mathcal{N}}} \theta_{\mathcal{N}}^j$  via (7);

**if**  $\Theta_{\mathcal{N}} = \emptyset$  **or**  $i > N_{uf}$  **then return**  $\theta$ .

**for**  $j = 1, \dots, N_{\mathcal{N}}$  **do**

    Initialize sub-trajectory  $\theta \leftarrow \theta_{\mathcal{N}}^j$  with  $\mathcal{GP}$ ;

**for** *PenIter* :  $1 \dots N_{\varrho}$  **do**

      Check the body-obstacle stuck according to Section IV-C.1;

**if** *isStuck* **then**

        | Optimize  $\theta$  via Algorithm 3;

**else**

        | Optimize  $\theta$  via Algorithm 2;

**if**  $\mathcal{F}_{obs}(\theta) < obstol$  **then**

        | **break**

**else**

        |  $\varrho \leftarrow \kappa_{\varrho} \cdot \varrho$ ;

    Update the factors of Bayesian tree;

---

where a smaller  $c_{\eta}$  filters out more factors. Then it regroups  $\Theta_{\mathcal{N}}$  into  $\Theta_{\mathcal{N}} = \bigcup_{j=1}^{N_{\mathcal{N}}} \theta_{\mathcal{N}}^j$  whose elements are sub-trajectory constructed by the adjacent factors  $\forall \theta_i \in \theta_{\mathcal{N}}^j$ . All sub-trajectories are optimized with the mixed steps in *reTrajIter* of Algorithm 1 and Figure 1. When  $\Theta_{\mathcal{N}}$  is optimized, iSAGO updates the Bayes tree and regenerates  $\Theta_{\mathcal{N}}^{j+1}$  for an incremental optimization. Note that  $\kappa_{\varrho}$  updates  $\varrho$  coincided with the sub-trajectory rather than the whole trajectory.

### B. Accelerated Gradient Descent for Optimization

This paper gathers the accelerated gradient information for trajectory optimization because it only requires the first

order momenta to achieve an optimal convergence [29] with Lipschitz continuous gradient

$$\mathcal{C}_{\theta} = \{\theta' \mid |\mathcal{F}(\theta') - \mathcal{F}(\theta) - \langle \bar{\nabla} \mathcal{F}(\theta), \theta' - \theta \rangle| \leq \frac{\mathcal{L}_{\mathcal{F}}}{2} \|\theta' - \theta\|^2\}. \quad (9)$$

In this way, we adopt the update rules:

$$\alpha_k = \frac{2}{k+1}, \quad \beta_k = \frac{1}{2\mathcal{L}_{\mathcal{F}}}, \quad \lambda_k = \frac{k\beta_k}{2}, \quad (10)$$

then for  $\forall n > 1$ , we have <sup>2</sup>

$$\min_{k=1 \dots n} \|\bar{\nabla} \mathcal{F}(\theta_k^{md})\|^2 \leq \frac{96\mathcal{L}_{\mathcal{F}} \|\theta^* - \theta_0\|^2}{n^2(n+1)}, \quad (11)$$

Some former studies [15], [16], [29] set a Lipschitz constant  $\mathcal{L}_{\mathcal{F}}$  for accelerated descent. However, (11) indicates a strong correlation between the super-linear convergence rate and  $\mathcal{L}_{\mathcal{F}}$ . Some studies [17], [30] introduce the restart schemes for speeding up when the problem is not globally convex. Algorithm 2 adopts the trust-region method [14] to adjust  $\mathcal{L}_{\mathcal{F}}$  with factor  $\tau_{\mathcal{L}}$  and restart AGD until the condition

$$|\mathcal{F}_k - \mathcal{F}_{k-1} - \langle \bar{\nabla} \mathcal{F}_k^{md}, \theta_k - \theta_{k-1} \rangle| \leq \frac{\mathcal{L}_{\mathcal{F}}}{2} \|\theta_k - \theta_{k-1}\|^2 \quad (12)$$

is satisfied. In this way, we only arbitrarily initialize  $\mathcal{L}_{\mathcal{F}}$  as  $\delta_0 \|\bar{\nabla}_{\theta} \mathcal{F}(\hat{\theta})\|$  and update it exponentially with  $\kappa_{\mathcal{L}}$  to approach first-order robust convergence.

---

### Algorithm 2: AGD

---

**Input** : Initial  $\theta_0$ , penalty  $\varrho$ , and  $\mathcal{GP}(\mu, \mathcal{K})$ .

**Initialization**:  $\bar{\nabla} \mathcal{F}_1^{md} = \bar{\nabla} \mathcal{F}_0$ ,  $\mathcal{L}_{\mathcal{F}} = \delta_0 \|\bar{\nabla} \mathcal{F}_0\|$ ;

**for** *LIter* :  $j = 1 \dots N_{\mathcal{L}}$  **do**

**for** *AgdIter* :  $k = 1 \dots N_{ag}$  **do**

$\theta_k^{md} = (1 - \alpha_k) \theta_{k-1}^{ag} + \alpha_k \theta_{k-1}$ ;

**if**  $k \geq 2$  **then**  $\bar{\nabla} \mathcal{F}_k^{md} \leftarrow \bar{\nabla} \mathcal{F}(\theta_k^{md})$ ;

    Update  $\alpha_k$ ,  $\beta_k$  and  $\lambda_k$  by (10);

$\theta_k = \theta_{k-1} - \lambda_k \bar{\nabla} \mathcal{F}_k^{md}$ ;

$\theta_k^{ag} = \theta_k^{md} - \beta_k \bar{\nabla} \mathcal{F}_k^{md}$ ;

**if** *Converge to  $\mathcal{F}tol$  or  $\theta tol$  or isStuck* **then**

      | **return**  $\theta_k^{md}$ .

**if** *condition (12) is not satisfied* **then**

      |  $\{\theta_0^{md}, \theta_0^{ag}, \theta_0\} \leftarrow \theta_{k-1}^{md}$ ;  $\mathcal{L}_{\mathcal{F}} \leftarrow \kappa_{\mathcal{L}} \cdot \mathcal{L}_{\mathcal{F}}$ ;

      |  $\bar{\nabla} \mathcal{F}_1^{md} \leftarrow \bar{\nabla} \mathcal{F}_{k-1}^{md}$ ; **break**

---

The above AGD keeps execution until it converges

$$|\mathcal{F}_k - \mathcal{F}_{k-1}| < \mathcal{F}tol, \quad \|\theta_k - \theta_{k-1}\| < \theta tol$$

or the stuck-case is detected according to Section IV-C.1.

<sup>2</sup>See more details in [16]: (a) Lemma 1 provides an analytic view of the damped descent of Ghadimi's AGD; (b) Theorem 1 provides AGD's convergence rate, and its proof validates the accelerated descent process.

### C. Stochastic Optimization with Momentum Adaptation

Some studies of deep learning [20], [21], [31], [32] propose stochastic gradient descent (SGD) for learning objects with noisy or sparse gradients. They optimize the objective function consisting of sub-functions in low coupling. Because of the higher robustness of Adam [20] during the function variation, we adopt its moment adaptation method and propose STOMA (Algorithm 3, Figure 2b) in the stuck case. This section will first illustrate how to detect the stuck case, generate the stochastic gradient (SG), and introduce how the SGD accelerated with moment adaptation.

---

#### Algorithm 3: STOMA

---

**Input:** Initial  $\theta_0$ ,  $\varrho$  and  $\mathcal{GP}(\mu, \mathcal{K})$

- 1 **for** *reSgdIter*:  $j = 1 \dots N_{rsg}$  **do**
- 2     Sample  $\Theta_K = \{\theta_k \sim \mathcal{GP}(\mu, \mathcal{K}) \mid_{k=1 \dots K}\}$ ;
- 3     Evaluate costs  $\mathfrak{F}_K = \{\mathcal{F}[\theta_1], \dots, \mathcal{F}[\theta_K]\}$ ;
- 4     Reinitialize  $\theta_0 = \operatorname{argmin}_{\theta \in \Theta_K} \mathfrak{F}_K$ ;
- 5     **for** *SgdIter*:  $k = 1 \dots N_{sg}$  **do**
- 6         Update  $N_{sg} \sim \mathcal{U}(N_{lo}^{sg}, N_{up}^{sg})$  randomly;
- 7          $\theta_k^{sg} = (1 - \alpha_k) \theta_{k-1}^{sg} + \alpha_k \theta_{k-1}$ ;
- 8         Compute  $\bar{\nabla} \mathcal{F}^{sg}(\theta_k^{sg})$  and check *stuck*-case;
- 9         **if not isStuck or**  $\|\theta_k - \theta_{k-1}\| \leq SGtol$  **or**  
            $j \geq N_{rsg}$  **then return**  $\theta_k^{sg}$ .
- 10         **if**  $k \geq N_{sg}$  **then**  $\{\theta_0^{sg}, \theta_0\} \leftarrow \theta_k^{sg}$ ; **break**
- 11         Estimate the 2<sup>nd</sup> moment  $\mathfrak{M}_k$  via (16);
- 12         Update  $\alpha_k$ ,  $\mathfrak{B}_k$  and  $\lambda_k$  via (17);
- 13          $\theta_k = \theta_{k-1} - \lambda_k \bar{\nabla} \mathcal{F}^{sg}(\theta_k^{sg})$ ;
- 14          $\theta_k^{sg} = \theta_k^{sg} - \mathfrak{B}_k \bar{\nabla} \mathcal{F}^{sg}(\theta_k^{sg})$ ;

---

#### 1) Stochastic gradient generation and Stuck case check:

Since (1) reveals that whole objective functional uses the penalty factor  $\varrho$  gather the GP prior and obstacle information which accumulates the sub-functions calculated by collision-check boxes (CCBs) in discrete time, we generate a SG in functional, time, and space:

$$\bar{\nabla} \mathcal{F}^{sg} = \varrho \bar{\nabla} \mathcal{F}_{gp} + \bar{\nabla} \mathcal{F}_{obs}^{sg}. \quad (13)$$

In the functional part, we select the penalty factor  $\frac{1}{\varrho} \sim \mathcal{U}(0, \frac{1}{\varrho})$ . In the time part, we select  $n_{t_i}^{ip} \sim \mathcal{U}(0, N^{ip})$ , the number of interval waypoints of any two support waypoints  $[\theta_{t_i}^\top, \theta_{t_{i+1}}^\top]^\top$ , to gain a sub-gradient for collision-check:

$$\bar{\nabla} \mathcal{F}_{obs}^{sg} = \mathbf{M}_{sg}^\top \cdot \mathbf{g}_{up}, \quad (14)$$

where  $\Lambda_{t_i}^{sg} = [\Lambda_{i,1}^\top \dots \Lambda_{i,n_{t_i}^{ip}}^\top]^\top$ ,  $\Psi_{t_i}^{sg} = [\Psi_{i,1}^\top \dots \Psi_{i,n_{t_i}^{ip}}^\top]^\top$  are gained according to (4)-(5), and a upsampling matrix

$$\mathbf{M}_{sg} = \begin{bmatrix} \mathbf{I} & \mathbf{0} & \mathbf{0} & \dots & \dots & \dots & \mathbf{0} & \mathbf{0} \\ \Lambda_t^{sg} & \Psi_t^{sg} & \mathbf{0} & \dots & \dots & \dots & \mathbf{0} & \mathbf{0} \\ \vdots & \vdots & \ddots & & & & \vdots & \vdots \\ \mathbf{0} & \mathbf{0} & \dots & \mathbf{I} & \mathbf{0} & \dots & \mathbf{0} & \mathbf{0} \\ \mathbf{0} & \mathbf{0} & \dots & \Lambda_{t_i}^{sg} & \Psi_{t_i}^{sg} & \dots & \mathbf{0} & \mathbf{0} \\ \mathbf{0} & \mathbf{0} & \dots & \mathbf{0} & \mathbf{I} & \dots & \mathbf{0} & \mathbf{0} \\ \vdots & \vdots & & & & & \vdots & \vdots \\ \mathbf{0} & \mathbf{0} & \dots & \dots & \dots & \dots & \Lambda_{t'/-1}^{sg} & \Psi_{t'/-1}^{sg} \\ \mathbf{0} & \mathbf{0} & \dots & \dots & \dots & \dots & \mathbf{0} & \mathbf{I} \end{bmatrix}$$

maps the upsampled gradient

$$\mathbf{g}_{up} = \begin{bmatrix} \nabla^\top \mathcal{F}_{obs}^{\mathcal{B}}[\theta(t)], \\ \nabla^\top \mathcal{F}_{obs}^{\mathcal{B}} \left[ \theta \left( t + \frac{1}{n_{t'}^{ip} + 1} \right) \right], \dots, \nabla^\top \mathcal{F}_{obs}^{\mathcal{B}}[\theta(t+1)], \\ \vdots \\ \nabla^\top \mathcal{F}_{obs}^{\mathcal{B}} \left[ \theta \left( t' - \frac{n_{t'/-1}^{ip}}{n_{t'/-1}^{ip} + 1} \right) \right], \dots, \nabla^\top \mathcal{F}_{obs}^{\mathcal{B}}[\theta(t')] \end{bmatrix}^\top$$

into the gradient  $\bar{\nabla} \mathcal{F}_{obs}^{sg}$  of the trajectory  $\theta(t, t')$ .

Unlike the stochastic rules in functional and time, the intuition of the space rule comes from the collision avoidance of a human arm in a bookshelf (Figure 2a). When a blindfolded participant stretches for an object in a bookshelf, he makes reflexes alternatively in response to the arm-obstacle collision. The arm parts in danger (orange/red balls) stimulate the reflexes via the exterior forces (orange arrows). The human arm's obstacle avoidance trajectory (black curve) indicates the collision risk rises from shoulder to hand.

In this way, we first reconstruct each rigid body of a tandem manipulator by the geometrically connected CCBs. Then we build each sub-problem (i.e., collision avoidance of individual CCB) from shoulder to end-effector, considering the collision-risk variation of a different body part. So  $\nabla \mathcal{F}_{obs}^{\mathcal{B}}$  is calculated by accumulating the CCB-gradients from  $\mathcal{B}_1$  close to shoulder up to  $\mathcal{B}_k$  close to end-effector:

$$\nabla \mathcal{F}_{obs}^{\mathcal{B}}[\theta(t)] = \sum_{\mathcal{B}_k \in \mathcal{B}} \nabla \mathcal{F}_{obs}^k[\theta(t)], \quad (15)$$

$$\nabla \mathcal{F}_{obs}^k = \sum_{\substack{\mathcal{B}_i \in \mathcal{B}_k \\ \phi_i < \phi_{tol}}} \nabla_{q_i} \mathcal{F}_{obs}, \quad \mathcal{B}_k = \{\mathcal{B}_1, \dots, \mathcal{B}_k\},$$

where  $q_i$  contains the joints actuating CCB- $\mathcal{B}_i$ , and  $\phi_i$  is the included angle between the  $\mathcal{B}_i$ -gradient  $\nabla_{q_i} \mathcal{F}_{obs}$  and the accumulated gradient  $\nabla \mathcal{F}_{obs}^{i-1}$  (from  $\mathcal{B}_1$  to  $\mathcal{B}_{i-1}$ ). When there exists a  $\phi_i > \phi_{tol}$ , we think a waypoint  $\theta(t)$  is stuck in an obstacle. In this way, (i) the space stochasticity will vanish when  $\phi_{tol} \rightarrow 180^\circ$ ; (ii) the random  $\phi_{tol}$  generates SG by stochastically rejecting the  $\nabla_{q_i} \mathcal{F}_{obs}$  with  $\phi_i > \phi_{tol}$ .

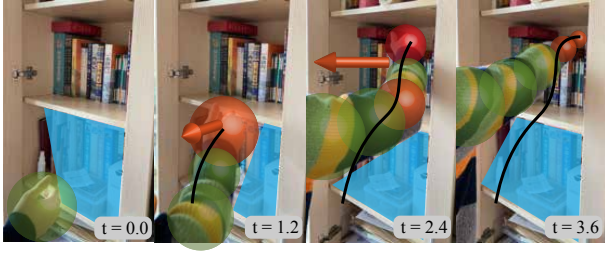
2) *Update rules:* Adam [20] adopts the piecewise production of gradients and uses EMA from the initial step up to the current step and the bias correction method for the adaptive momentum estimation. In our work, we use the squared  $\ell_2$ -norm of SG to estimate  $\hat{\mathfrak{M}}_1 = \|\bar{\nabla} \mathcal{F}_1^{sg}\|^2$ , and adopt EMA and bias correction for 2nd-momenta  $\{\mathfrak{M}_k\}$  estimation:

$$\hat{\mathfrak{M}}_k = \gamma \hat{\mathfrak{M}}_{k-1} + (1-\gamma) \bar{\nabla} \mathcal{F}^{sg}(\theta_k^{sg})^{\odot 2}, \quad \mathfrak{M}_k = \frac{\hat{\mathfrak{M}}_k}{1-\gamma^k}. \quad (16)$$

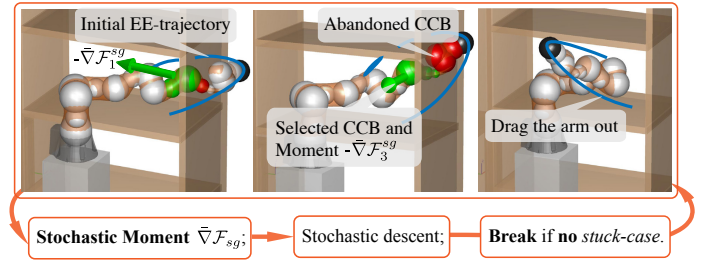
As shown in Algorithm 3, we adopt the AGD rules [16] rather than the EMA with bias correction for first-momentum adaptation. And  $\{\alpha_k, \mathfrak{B}_k, \lambda_k\}$ 's update rules are reset as

$$\alpha_k = \frac{2}{k+1}, \quad \mathfrak{B}_k = \frac{\mathfrak{M}_k^{-\frac{1}{2}}}{2\delta}, \quad \frac{\lambda_k}{|\mathfrak{B}_k|} \in \left[ 1, 1 + \frac{\alpha_k}{4} \right]. \quad (17)$$

In this way, the descent process, approximately bounded by a  $\delta$ -sized trust-region, accelerates via the  $\alpha$ -linear interpretation between the conservative step and the accelerated step driven by  $\{\lambda_k\}$  and  $\{\mathfrak{B}_k\}$  correspondingly. Then the process varies from the lag state guided by  $\theta$  to the shifting



(a) A series of frames illustrate how the human arm reacts to obstacles when grasping inside a bookshelf. The green, orange, and red balls show the none, low and high-risk areas of collision, respectively.



(b) STOMA (Algorithm 3) drags the robot-arm out of the body-obstacle interference via adaptive stochastic descent. The green CCBs are selected for stochastic momenta (green arrow) while the red ones are abandoned.

Fig. 2: From human-arm avoidance to robot-arm dragging

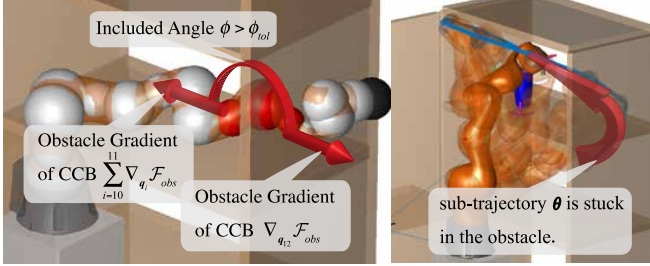


Fig. 3: The grey collision-check boxes (CCBs) assembly presents an LBR-iiwa, and the red box denotes the collision case. The stuck case happens when the included angle  $\phi > \phi_{tol}$ .

one guided by  $\theta^{ag}$  with  $\{\alpha_k\}$  value. Since the SGD is roughly Lipschitz continuous, we get

$$\begin{aligned} \mathcal{F}_{k-1} &\leq \mathcal{F}_k + \langle \bar{\nabla} \mathcal{F}_{k-1}, \theta_k - \theta_{k-1} \rangle \\ &\leq \mathcal{F}_k + \lambda_k \|\bar{\nabla} \mathcal{F}_k^{sg}\|^2 + \lambda_k \|\Delta_k\| \|\bar{\nabla} \mathcal{F}_k^{sg}\|, \end{aligned}$$

where  $\mathcal{F}_k$  and  $\mathcal{F}_k^{sg}$  simplify  $\mathcal{F}(\theta_k)$  and  $\mathcal{F}(\theta_k^{sg})$ , and

$$\|\Delta_k\| = \|\bar{\nabla} \mathcal{F}_{k-1} - \bar{\nabla} \mathcal{F}_k^{sg}\| \leq \mathcal{L}_{\mathcal{F}}^{sg} (1 - \alpha_k) \|\theta_{k-1}^{ag} - \theta_{k-1}\|,$$

$$\theta_k^{ag} - \theta_k = (1 - \alpha_k) (\theta_{k-1}^{ag} - \theta_{k-1}) + (\lambda_k - \beta_k) \bar{\nabla} \mathcal{F}_k^{sg}$$

according to Algorithm 3 (line 7, 13, 14). Combining the Cauchy-Schwarz inequation, we get

$$\begin{aligned} \mathcal{F}_{k-1} &\leq \mathcal{F}_k + \lambda_k \left(1 + \frac{\mathcal{L}_{\mathcal{F}}^{sg} \lambda_k}{2}\right) \|\bar{\nabla} \mathcal{F}_k^{sg}\|^2 \\ &\quad + \mathcal{L}_{\mathcal{F}} (1 - \alpha_k)^2 \frac{\|\theta_{k-1}^{ag} - \theta_{k-1}\|^2}{2}. \end{aligned}$$

Then through the accumulation from  $k = 1$  to  $N$ , we get

$$\frac{\mathcal{F}_0 - \mathcal{F}_N}{\mathcal{L}_{\mathcal{F}}^{sg}} \leq \sum_{k=1}^N \left( \lambda_k + \frac{\lambda_k^2}{2} + \frac{(\lambda_k - \beta_k)^2}{2\Gamma_k \alpha_k} \sum_{l=k}^N \Gamma_l \right) \|\bar{\nabla} \mathcal{F}_k^{sg}\|^2$$

where  $\beta_k = |\beta_k|_{\infty}$ ,  $\Gamma_l = (1 - \alpha_l) \Gamma_{l-1}$  with  $\Gamma_0 = 1$ .

In sight of the stochasticity of  $\mathcal{F}(\theta^{sg})$  and its gradient  $\bar{\nabla} \mathcal{F}(\theta^{sg})$  and presuming  $\|\bar{\nabla} \mathcal{F}_k\|_{c_l} \cdot \delta \geq \mathcal{L}_{\mathcal{F}}^{sg}$ , we get:

$$\frac{\mathcal{F}_0 - \mathcal{F}_N}{N} \leq \frac{5\mathbf{G}_{\infty}}{4\delta} \left(1 + \frac{11c_l}{32}\right) \frac{\ln(N+1)}{N}, \quad (18)$$

where  $c_l$  is the fraction of  $\mathcal{L}_{\mathcal{F}}$  and trust region box  $\delta \cdot \|\bar{\nabla} \mathcal{F}_k\|$ , and  $\mathbf{G}_{\infty} \leq \mathbb{E}(\|\bar{\nabla}^{\top} \mathcal{F}_1^{sg}, \dots, \bar{\nabla}^{\top} \mathcal{F}_N^{sg}\|_{\infty})$ .

Figure 2b illustrates how a robot reflexes to the stuck case like the human in Figure 2a following the update rules in *SgdIter*. To improve the computational efficiency and success

rate, we nest the above process (i.e., *SgdIter*) in *reSgdIter*. Once *SgdIter* restarts, we select the trajectory with the lowest functional cost from the sampled set  $\Theta_K$  to reinitialize the trajectory for the following stochastic optimization in *SgdIter*. The maximum number  $N_{sg}$  of *SgdIter* is selected randomly in  $[N_{lo}^{sg}, N_{up}^{sg}]$ .

## V. EXPERIMENT

This section will first introduce constructing the objective functional in Section V-A. Then it will detail the benchmark and parameter setting in Section V-B.1 & V-B.2 and analyze the benchmark results in Section V-B.3.

### A. Implementation details

1) *GP prior*: To decrease the state-space dimension, we assume the joint velocity is constant and gain the Gauss-Markov model and GP prior [2]. Moreover, our benchmark<sup>3</sup> uses 12 support states with 8 intervals (116 states in total) for iSAGO and GPMP2, 116 states for STOMP and CHOMP, 12 and 58 states for TrajOpt, and MaxConnection-Distance =  $\frac{\|\theta_g - \theta_0\|}{12}$  for RRT-Connect.

2) *Collision cost function*: Our work adopts the polynomial piecewise form of [1] for the collision cost function.

3) *Motion constraints*: The motion cost function in GPMP [2] is adopted to drive the robot under the preplanned optimal collision-free trajectory in the real world.

### B. Evaluation

1) *Setup for benchmark*: This paper benchmarks iSAGO against the numerical planners (CHOMP [1], TrajOpt [3], GPMP2 [2]) as well as the sampling-based planners (STOMP [8], RRT-Connect [7]) on a 7-DoF robot (LBR-iiwa) and a 6-DoF robot (AUBO-i5). Since the benchmark executes in MATLAB, we install the compiled GPMP2-toolbox and use BatchTrajOptimize3DArm to implement GPMP2 [2] and use planarBiRRT to implement RRT-Connect [7]. TrajOpt is an SCO with the trust-region method internally using Gurobi. So our benchmark uses fmincon with options =

<sup>3</sup>Since TrajOpt proposes a swept-out area between support waypoints for time-continuous safety, we choose TrajOpt-12 for safety validation and TrajOpt-58 to ensure the dimensional consistency of the benchmark.

optimoptions('fmincon','Algorithm','trust-region-reflective','SpecifyObjectiveGradient',true), which calculates ObjectiveGradient analytically and Aeq (the matrix whose rows are the active constraint gradients) via numerical differentiation like TrajOpt. Since CHOMP adopts HMC for optimal trajectory and momentum, our benchmark defines an hmcSampler object whose logarithm probabilistic density function (logpdf) is defined as (1), uses hmcSampler.drawSamples for HMC, and compiles it in CMex-file. As for STOMP, our benchmark uses mvnrnd for noise trajectories sampling and updates the trajectory via projected weighted averaging [8].

To illustrate the competence of iSAGO for planning tasks, we conduct 25 experiments on LBR-iiwa at a bookshelf and 12 experiments on AUBO-i5 at a storage shelf. We categorize all tasks into 3 classes (A, B, and C, Figure 4) whose planning difficulty rises with the stuck cases in the initial trajectory increase. Considering the difficulty of different classes, we first generate 2 tasks of class A, 3 tasks of class B, and 4 tasks of class C for LBR-iiwa (Figures 4a-4f). Then we generate 6 tasks of class C for AUBO-i5 (Figures 4g-4l). Each task consists of 2 to 4 problems<sup>4,5</sup> with the same initial state and goal constraint. Moreover, we compare iSAGO with SAGO to show the efficiency of the incremental method and compare SAGO with STOMA or AGD to show the efficiency and reliability of the mixed optimization.

2) *Parameter setting*: Since STOMA (Algorithm 3, Figure 2b) proceeds SGD roughly contained in a  $\delta$ -sized trust-region with  $\gamma$ -damped EMA of historical momenta, this section first tunes these two parameters, then the others.

According to abundant experiences, we tune the key parameters around  $\{\delta = 0.80, \gamma = 0.90\}$ . We conduct 10 different C-class tasks when tuning  $\{\delta, \gamma\}$  and estimate the 95% confidence interval of the SGD's expectation. Each sub-figure of Figure 6 illustrates 10 SGDs and their confidence interval denoted by the purple area under the specific  $\{\delta, \gamma\}$ . The larger interval of  $\delta = 0.80$  indicates the lower robustness of SGD, meaning the unstable iSAGO, while the higher SGD-rate of  $\gamma = 0.99$  indicates the higher efficiency. We statistically analyze the results under variant  $\delta \in [0.04, 0.80]$  and  $\gamma \in [0.50, 0.99]$  to demonstrate the key parameter tuning further. Table I ('(%)' and '(s)') indicates the SGD-rate increases with  $\delta$ -expansion. In contrast, the success rate decreases with the excessive  $\delta$  (i.e., too high or too low). Moreover, the SGD-rate increases with  $\gamma$ -shrink while the success rate decreases with  $\gamma$ -shrink. So we finally choose  $\delta = 0.40$  and  $\gamma = 0.90$ .

Besides  $\delta$  and  $\gamma$ , we set the initial penalty  $\varrho = 1.25e-2$  and penalty factor  $\tau_c = 0.4$  in Algorithm 1. In Algorithm 2,

<sup>4</sup>Since LBR-iiwa has 7 DoFs, meaning infinite solutions for the same goal constraint, our benchmark uses LM [13] with random initial points to generate different goal states. So one planning task of LBR-iiwa with the same goal-constraint has several problems with different goal states.

<sup>5</sup>Since the same goal constraint has only one solution for AUBO-i5 with 6 DoFs and we set the yaw-angle as  $0^\circ$  or  $180^\circ$ , each task has two problems with the same initial state and goal constraint.

TABLE I: Results for  $\{\delta, \gamma\}$  tuning of 10 tasks in class C

$\begin{matrix} (\%)(s) \\ \gamma \end{matrix} \backslash \delta$	0.80	0.40	0.08	0.04
0.50	80   1.253	90   1.898	60   4.198	40   6.309
0.90	90   2.512	<b>100   2.463</b>	80   4.973	60   8.219
0.99	90   2.672	<b>100   3.089</b>	80   7.131	60   12.57

we set the threshold or tolerance  $c_l = 0.1$ ,  $c_u = 0.9$ ,  $\mathcal{F}tol = 8e-4$ ,  $\theta tol = 10^{-3}$ , and the arbitrary Lipschitz factor  $\tau_{\mathcal{L}} = 6.67$ . In Algorithm 3, we set the number of samples and the selected samples as  $K = 12$  and  $M = 6$  respectively, tolerance  $SGtol = 6.4e-3$ ,  $ImpRtol = 0$ , and generate  $N_{sg} \sim \mathcal{U}(35, 55)$ . Moreover, we select  $\phi_{tol} = 95^\circ$  for stuck case check and generate the stochastic momenta by selecting  $\phi_{tol} \sim \mathcal{U}(60^\circ, 180^\circ)$ . Finally, we choose  $\epsilon = 0.05$  for collision check and  $\epsilon = 0.01$  for motion constraints.

3) *Results analysis*: The successful results in Figure 5 guide the iiwa arm to actuate safely with high smoothness in the narrow workspace. Tables II & III both show that iSAGO gains the highest success rate compared to the others. The random *SgdIter* number  $N_{sg}$  and AGD help iSAGO gain the fourth solving rate after TrajOpt-12, TrajOpt-58, and GPMP2-12. Though TrajOpt-58 compensates for the continuous safety information leak in TrajOpt-12, it still cannot escape from the local minima arising from SCO (trust-region) and gains the second lowest success rate just above TrajOpt-12. However, iSAGO successfully descends into an optimum with adaptive stochastic momenta and a proper trust-region. Thanks to HMC, randomly gaining the Hamiltonian momentum, CHOMP approaches the optimum with the third-highest success rate, whose failures are informed by the exact momenta rather than the adaptive stochastic momenta. RRT-Connect has the second-highest success rate despite the largest computation resource for RRT growing restricted by `MaxConnectionDistance`, negatively affecting success rate. Though STOMP is free of gradient calculation, the significant times it takes to resample do a minor effect for feasible searching, mainly limited by the Gaussian covariance. As for GPMP2-12 and TrajOpt-58, the LM method and the trust-region method help them approach the stationary point rapidly, while whether the point is feasible highly depends on the initial.

The comparison between STOMA and SAGO in Tables II & III shows how AGD performs a 45% accelerated descent towards an optimum. The comparison between iSAGO and SAGO indicates a 55% higher efficiency of the incremental planning. The 90% lower success rate of AGD than SAGO shows the limitation of the numerical method. It validates that STOMA can modify the manifold with less local minima by the random selection of sub-functional.

The comparison between Tables II & III shows that iSAGO performs better when the feasible solution is nearby the motion constraints. That is because the motion constraint somewhat stabilizes the  $\delta$ -sized SGD of STOMA. So the arbitrary SGD-steps with a large  $\delta$  bring the severe disturbance of stochastic momenta and weaken the STOMA's perfor-

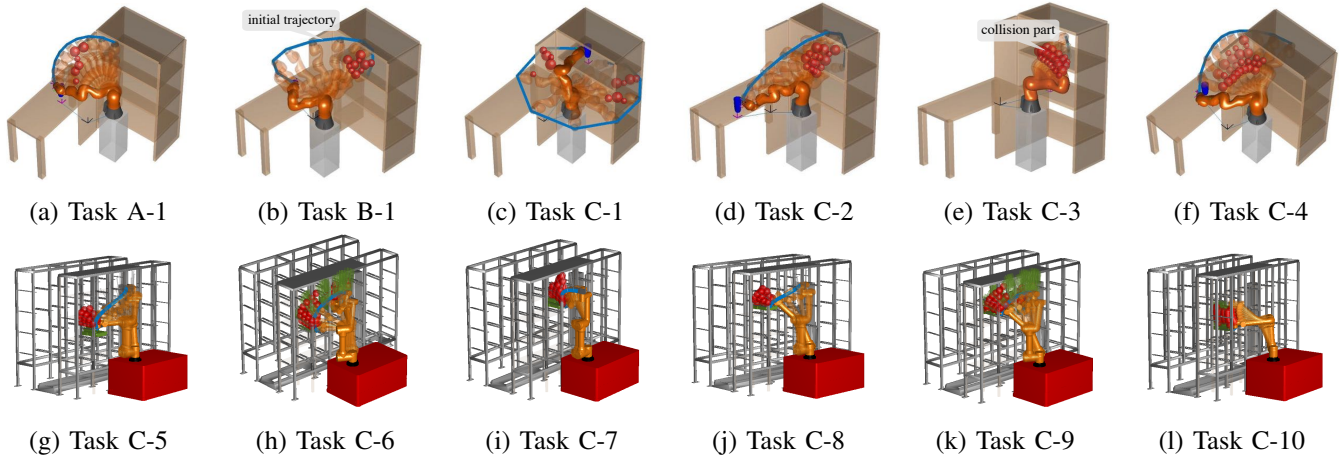


Fig. 4: The initial trajectory with red boxes (collision parts) visualizes our benchmark on LBR-iiwa and AUBO-i5. *Task C-9* means No.9 task of class C.

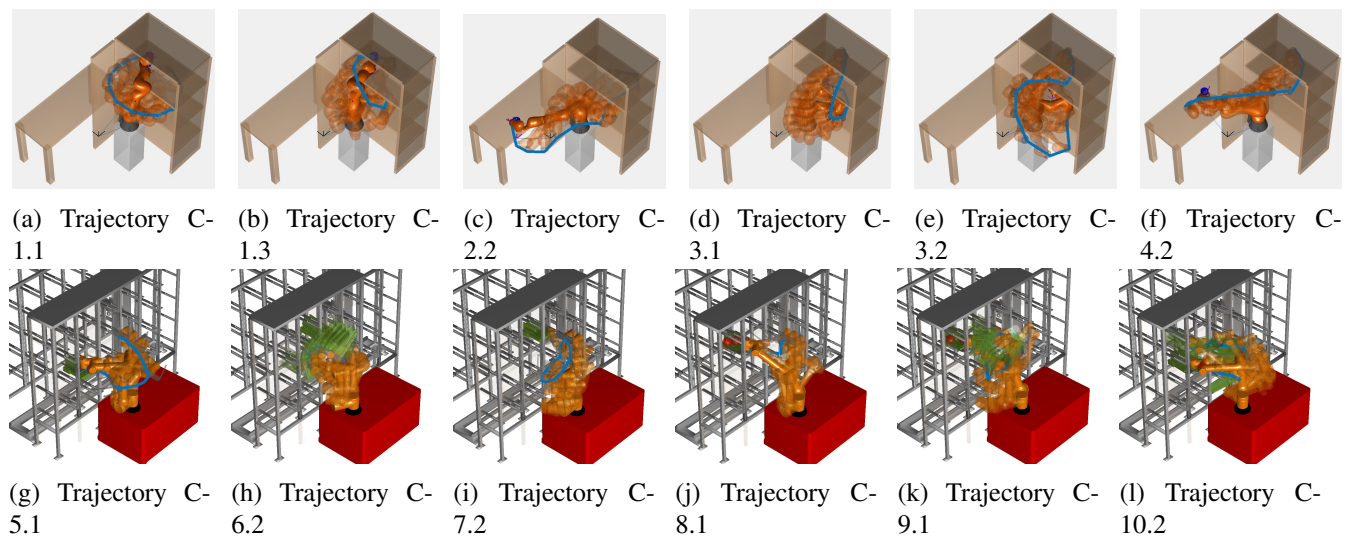


Fig. 5: Some results of iSAGO in class C (*Trajectory C-1.3* means the 3rd planning result of task 1 in class C. )

TABLE II: Results for 16 planning tasks with 5 repeated tests for LBR-iiwa in class C

	Our incremental mixed optimization				numerical optimization				probabilistic sampling	
	AGD	STOMA	SAGO	iSAGO	TrajOpt-12	TrajOpt-58	GPMP2-12	CHOMP	STOMP	RRT-Connect
Suc. Rate (%)	8.75	87.5	91.25	<b>93.75</b>	3.75	8.75	11.25	30	25	72.5
Avg. Time (s)	0.288	7.622	4.284	2.132	<b>0.232</b>	1.108	2.464	6.989	7.691	13.65
Std-Dev. Time (s)	0.045	1.735	1.048	0.319	<b>0.055</b>	0.101	1.312	1.290	5.233	4.562

TABLE III: Results for 12 planning tasks with 5 repeated tests for AUBO-i5 in class C

	AGD	STOMA	SAGO	iSAGO	TrajOpt-12	TrajOpt-58	GPMP2-12	CHOMP	STOMP	RRT-Connect
Suc. Rate (%)	5	71.67	83.33	<b>88.33</b>	3.33	6.67	11.67	26.67	25	73.33
Avg. Time (s)	0.343	8.584	4.812	2.413	<b>0.245</b>	1.119	2.610	7.588	8.640	16.02
Std-Dev. Time (s)	0.078	1.821	1.101	0.334	<b>0.057</b>	0.106	1.377	1.354	5.494	3.974

mance by 20% when obstacles wrap the optimal trajectory.

## VI. CONCLUSIONS

iSAGO utilizes the mixed information of accelerated (AGD) and stochastic (STOMA) momentum to overcome the body-obstacle stuck cases in a narrow workspace.

(1) STOMA performs an adaptive stochastic descent to avoid the local minima confronted by the numerical methods, such as CHOMP, GPMP, and TrajOpt. The results show it gains the highest success rate of the numerical methods.

(2) AGD integrated by iSAGO accelerates the descent informed by the first-order momenta. The results show it

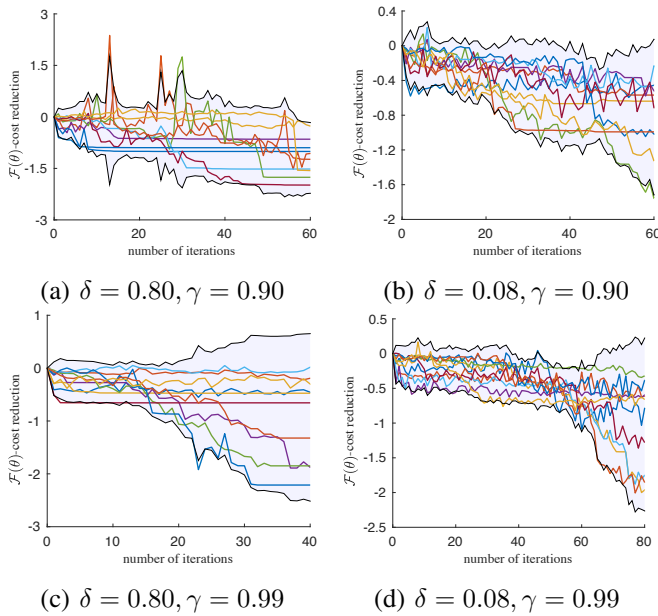


Fig. 6: The result of  $\delta, \gamma$  adjustment

saves the sampling method's computation resources and gain the fourth solving rate.

(3) The incremental planning optimizes the sub-planning to elevate the whole-planning rate further. The results show the 55% higher efficiency of iSAGO than SAGO.

#### ACKNOWLEDGMENT

The work of this paper is supported by the National Natural Science Foundation of China (No. 52175032), the Key R&D Program of Zhejiang Province (2020C01025, 2020C01026), and Robotics Institute of Zhejiang University Grant (K11808).

#### References

- [1] M. Zucker, N. Ratliff, A. D. Dragan, M. Pivtoraiko, M. Klingensmith, C. M. Dellin, J. A. Bagnell, and S. S. Srinivasa, "Chomp: Covariant hamiltonian optimization for motion planning," *The International Journal of Robotics Research*, vol. 32, no. 9-10, pp. 1164–1193, 2013.
- [2] M. Mukadam, J. Dong, X. Yan, F. Dellaert, and B. Boots, "Continuous-time gaussian process motion planning via probabilistic inference," *The International Journal of Robotics Research*, vol. 37, no. 11, pp. 1319–1340, 2018.
- [3] J. Schulman, J. Ho, A. X. Lee, I. Awwal, H. Bradlow, and P. Abbeel, "Finding locally optimal, collision-free trajectories with sequential convex optimization." in *Robotics: science and systems*, vol. 9, no. 1. Citeseer, 2013, pp. 1–10.
- [4] M. Bhardwaj, B. Boots, and M. Mukadam, "Differentiable gaussian process motion planning," in *2020 IEEE International Conference on Robotics and Automation (ICRA)*, May 2020, pp. 10598–10604.
- [5] L. E. Kavraki, M. N. Kolountzakis, and J. . Latombe, "Analysis of probabilistic roadmaps for path planning," *IEEE Transactions on Robotics and Automation*, vol. 14, no. 1, pp. 166–171, Feb 1998.
- [6] S. M. LaValle *et al.*, "Rapidly-exploring random trees: A new tool for path planning," 1998.
- [7] J. J. Kuffner and S. M. LaValle, "Rrt-connect: An efficient approach to single-query path planning," in *Proceedings 2000 ICRA. Millennium Conference. IEEE International Conference on Robotics and Automation. Symposia Proceedings (Cat. No.00CH37065)*, vol. 2, April 2000, pp. 995–1001 vol.2.
- [8] M. Kalakrishnan, S. Chitta, E. Theodorou, P. Pastor, and S. Schaal, "Stomp: Stochastic trajectory optimization for motion planning," in *2011 IEEE International Conference on Robotics and Automation*, May 2011, pp. 4569–4574.
- [9] S. Karaman and E. Frazzoli, "Sampling-based algorithms for optimal motion planning," *The international journal of robotics research*, vol. 30, no. 7, pp. 846–894, 2011.
- [10] P. Rajendran, S. Thakar, A. M. Kabir, B. C. Shah, and S. K. Gupta, "Context-dependent search for generating paths for redundant manipulators in cluttered environments," in *2019 IEEE/RSJ International Conference on Intelligent Robots and Systems (IROS)*, 2019, pp. 5573–5579.
- [11] K. Shirley, "Inference from simulations and monitoring convergence," *Handbook of Markov Chain Monte Carlo*, May 2011.
- [12] M. Kaess, H. Johannsson, R. Roberts, V. Ila, J. J. Leonard, and F. Dellaert, "isam2: Incremental smoothing and mapping using the bayes tree," *The International Journal of Robotics Research*, vol. 31, no. 2, pp. 216–235, 2012.
- [13] K. Levenberg, "A method for the solution of certain non-linear problems in least squares," *Quarterly of Applied Mathematics*, vol. 2, no. 2, pp. 164–168, 1944.
- [14] R. H. Byrd, J. C. Gilbert, and J. Nocedal, "A trust region method based on interior point techniques for nonlinear programming," *Mathematical programming*, vol. 89, no. 1, pp. 149–185, 2000.
- [15] Y. Nesterov, "A method for unconstrained convex minimization problem with the rate of convergence  $o(1/k^2)$ ," in *Doklady an ussr*, vol. 269, 1983, pp. 543–547.
- [16] S. Ghadimi and G. Lan, "Accelerated gradient methods for nonconvex nonlinear and stochastic programming," *Mathematical Programming*, vol. 156, no. 1-2, pp. 59–99, 2016.
- [17] W. Su, S. Boyd, and E. Candes, "A differential equation for modeling nesterov's accelerated gradient method: Theory and insights," in *Advances in Neural Information Processing Systems 27*, Z. Ghahramani, M. Welling, C. Cortes, N. D. Lawrence, and K. Q. Weinberger, Eds. Curran Associates, Inc., 2014, pp. 2510–2518.
- [18] A. C. Wilson, B. Recht, and M. I. Jordan, "A Lyapunov analysis of momentum methods in optimization," 2018.
- [19] L. Bottou, "Large-scale machine learning with stochastic gradient descent," in *Proceedings of COMPSTAT'2010*, Y. Lechevallier and G. Saporta, Eds. Heidelberg: Physica-Verlag HD, 2010, pp. 177–186.
- [20] D. P. Kingma and J. Ba, "Adam: A method for stochastic optimization," *arXiv preprint arXiv:1412.6980*, 2014.
- [21] H. Geoffrey, N. Srivastava, and K. Swersky, "Neural networks for machine learning lecture 6a overview of mini-batch gradient descent," Department of Computer Science, University of Toronto, Tech. Rep. 14, 02 2012.
- [22] X. Wu and M. W. Mueller, "In-flight range optimization of multi-copters using multivariable extremum seeking with adaptive step size," in *2020 IEEE/RSJ International Conference on Intelligent Robots and Systems (IROS)*, 2020, pp. 1545–1550.
- [23] K. Solovey, O. Salzman, and D. Halperin, "New perspective on sampling-based motion planning via random geometric graphs," *The International Journal of Robotics Research*, vol. 37, no. 10, pp. 1117–1133, 2018.
- [24] E. W. Dijkstra, "A note on two problems in connexion with graphs," *Numerische Mathematik*, vol. 1, no. 1, pp. 269–271, 1959.
- [25] A. G. Hofmann, E. Fernandez, J. Helbert, S. D. Smith, and B. C. Williams, "Reactive integrated motion planning and execution," in *Twenty-Fourth International Joint Conference on Artificial Intelligence*, 2015.
- [26] L. Petrović, J. Peršić, M. Seder, and I. Marković, "Stochastic optimization for trajectory planning with heteroscedastic gaussian processes," in *2019 European Conference on Mobile Robots (ECMR)*, 2019, pp. 1–6.
- [27] T. Osa, "Multimodal trajectory optimization for motion planning," *The International Journal of Robotics Research*, vol. 39, no. 8, pp. 983–1001, 2020.
- [28] J. Nocedal and S. Wright, *Numerical optimization*. Springer Science & Business Media, 2006.
- [29] Y. Nesterov, *Introductory lectures on convex optimization: A basic course*. Springer Science & Business Media, 2013, vol. 87.
- [30] B. O'Donoghue and E. Candès, "Adaptive restart for accelerated gradient schemes," *Foundations of Computational Mathematics*, vol. 15, no. 3, pp. 715–732, 2015.



- [31] J. Duchi, E. Hazan, and Y. Singer, "Adaptive subgradient methods for online learning and stochastic optimization," *J. Mach. Learn. Res.*, vol. 12, pp. 2121–2159, July 2011.
- [32] I. Goodfellow, Y. Bengio, and A. Courville, *Deep learning*. MIT press, 2016.